

Role of symmetries in the transition to turbulence in optics

Jorge Farjas, Daniel Hennequin, Didier Dangoisse, and Pierre Glorieux

Laboratoire de Spectroscopie Hertzienne, Unité Associée au Centre National de la Recherche Scientifique, CERLA, Bâtiment P5, Université des Sciences et Technologies de Lille, F-59655 Villeneuve d'Ascq Cedex, France

(Received 25 April 1997)

Spatiotemporal dynamics of patterns of the light beam emitted by a photorefractive oscillator has been investigated in the case of very large transverse dimensions. Time and space averagings show that the transition to turbulence as transverse dimensions are increased is a two-step process. Symmetry properties of the average patterns reveal that after the first transition from a boundary- to a bulk-dominated behavior already observed at Fresnel numbers $\mathcal{N}_F \approx 20$ there is a second transition around $\mathcal{N}_F \approx 100$. The regime corresponds to a complete loss of symmetry and appears here as soon as the correlation length of the patterns becomes of the same size as the period of the optical grating in the gain medium. [S1050-2947(98)01601-1]

PACS number(s): 42.65.Sf, 42.60.Jf

The domain of purely temporal nonlinear dynamics is now widely explored, but as spatial degrees of freedom are introduced, the level of complexity drastically increases and there remain wide fields to be explored both theoretically and experimentally. A possible approach is to expand the space-time evolution onto a suitable basis of modes such as the Karhunen-Loewe functions, or in optics the Gaussian modes, and thus to reduce the problem to high-dimensional temporal dynamics. When the number of dimensions increases, this approach becomes inefficient and different tools are required to describe and understand the complexity. On the theoretical side, this is the domain where amplitude equations are used to predict the patterns appearing in systems with very large transverse cross sections (i.e., very large aspect ratios) such as convection in hydrodynamics or lasers in optics [1]. In the transition from low- to high-dimensional chaos, the patterns evolve from a boundary-dominated self-organization to a bulk one that has its intrinsic time and space scales. Up to now, the related experimental studies used mostly statistical methods such as calculations of the spatiotemporal correlations of the patterns or analysis of the spatial charge distribution of phase singularities [2]. A main drawback of these statistical methods is that they are blind to the symmetry properties, while symmetries play a main role in the dynamics of such systems [3,5]. It was recently demonstrated that inside the domain of high-dimensional dynamics, time averaging restores the underlying symmetry that was lost in instantaneous patterns [4,5]. We show here that using this tool, the concepts of boundary and bulk behaviors have to be refined, taking into account the symmetries of the system, especially when several symmetries are competing in the problem.

If a system belongs to a given symmetry group, its behavior belongs to this group or to one of its subgroups. In other words, once the parameters acting on the system symmetry are fixed, the other control parameters may change the pattern symmetry, often through temporal bifurcations, such as Hopf ones [3]. Such transitions between symmetry subgroups were observed, e.g., in patterns emitted by low-dimensional lasers [3]. When several symmetries compete in the system, their relative influence may evolve as its aspect ratios increase. To clarify this point, we have studied the

behavior of an optical oscillator with photorefractive gain (OPG) where a boundary symmetry σ_0 and a bulk symmetry σ_u compete. We show that as the aspect ratios increase, σ_0 and σ_u cease successively, not simultaneously, to play a role in the dynamics. This route leads eventually to a regime of turbulence independent of any symmetry.

The experimental setup consists in an optical ring cavity of length L containing a 1-cm-long BSO ($\text{Bi}_{12}\text{SiO}_{20}$) photorefractive crystal pumped with 532-nm radiation (Fig. 1). The pump is provided by a Nd^{3+} YAG laser (where YAG denotes yttrium aluminum garnet), with an intensity of 15 mW at the input of the crystal and an angle θ with respect to the cavity propagation axis. The gain is provided through two-wave mixing between the pump and the cavity fields. The gain value depends drastically on θ and on the dc electric field E_{dc} applied transversally to the crystal. The results presented in the following have been obtained for $\theta = 1.5^\circ$ and $E_{dc} = 10^6$ V/m, resulting in a gain of typically 10 cm^{-1} . The cavity is closed with three plane mirrors and a beam splitter that extracts 10% of the beam intensity from the cavity. A lens stabilizes the cavity. It is located at the opposite side of the crystal, so that the waist of the intracavity beam lies inside the crystal. Its focal length f is chosen according to the desired cavity and beam characteristics. The former is

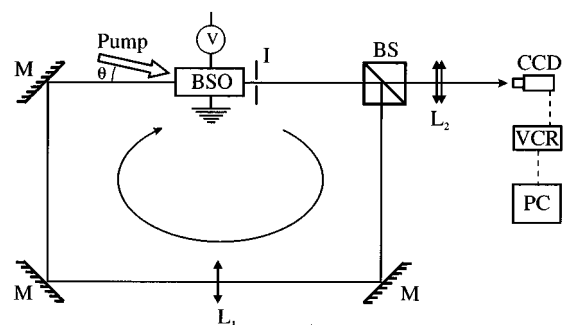


FIG. 1. Schematic experimental setup. M indicates a mirror, BS a beam splitter, and L_1 the intracavity lens. A voltage V is applied to the crystal. L_2 is a group of lenses that image the iris plane on the CCD camera. The video camera recorder (VCR) is connected to a computer (PC).

essentially determined by the ratio R_ν of the free spectral range $\Delta\nu_L$ and the transverse mode spacing $\Delta\nu_T$,

$$R_\nu = \frac{\Delta\nu_L}{\Delta\nu_T} = \frac{\pi}{\cos^{-1} \sqrt{1 - \frac{L}{4f}}},$$

while the latter is given by the beam waist value w_0 ,

$$w_0 = \sqrt{\frac{\lambda}{2\pi} \sqrt{L(4f-L)}},$$

where λ is the wavelength of the beam. For example, typical values of $f=0.8$ m and $L=2.4$ m lead to $\Delta\nu_L=125$ MHz, $R_\nu=3$, and $w_0=0.34$ mm.

An iris is inserted in the optical cavity to control σ_0 and the transverse size of the system. It is located 6 cm from the crystal, in the near field area, since the Rayleigh length of the intracavity beam is 68 cm for the typical cavity characteristics given above, and never decreases below 50 cm in our experimental setup. A video camera recorder (VCR) monitors the near-field image of the transverse distribution of the beam. We have checked that the patterns inside the crystal and in the plane of the iris are identical, and only patterns located in the iris plane are reported in the following. Temporal sequences have been recorded on a high-resolution video recorder so that the resolution of analogic pictures is typically 650×450 . Note that this number does not limit the resolution of the detection, as it is easy to record only one part of the pattern as a whole picture: This technique has been used to detect the pattern fine structures and, when necessary, to make the analyses. The acquisition frequency of such a system is 25 frames per second. A fast pointwise detector recording the global pattern intensity allows us to monitor continuously the main frequencies of the pattern evolution and incidentally to check that no evolution occurs at frequency above 10 Hz. Temporal averages have been obtained from these video recordings, using a computer digitizing one by one the frames stored in the VCR. Averages are always made on time length much larger than the main periods of the patterns, typically 10–100 times these periods, in conditions where the averages are independent of the number of pictures.

The transverse size of the optical cavity is measured through the generalized Fresnel number \mathcal{N}_F , which is the equivalent of the aspect ratio in hydrodynamics:

$$\mathcal{N}_F = \left(\frac{l_i}{w_i} \right)_{\min}^2.$$

l_i and w_i are the transverse radii of the cavity optical elements and of the beam measured at the same location in the cavity and along the i axis. The minimum value reached by this ratio all along the cavity is used for the evaluation of \mathcal{N}_F . Depending on the transverse symmetry of the cavity, this ratio may be different for each symmetry axis, as, e.g., in the case of a rectangular cavity: Therefore, \mathcal{N}_F has as many components as the cavity symmetry has main axes, as indicated by the indices i . The main difference between \mathcal{N}_F and the hydrodynamical aspect ratios is the square in the expres-

sion of the former. The origin of this square factor is that the empty cavity mode transverse size grows as the square root of its global index. In the present experimental setup, the mirrors and the beam splitter have a transverse diameter of 2.5 cm and the lens is 5 cm wide, while the crystal is 8 mm wide and is therefore the most limiting element in the absence of an iris. For the typical cavity characteristics given above, the spot sizes of the beam at the mirror further from the waist, at the lens, and in the crystal are, respectively, 0.56 mm, 0.69 mm, and 0.34 mm, leading to a local \mathcal{N}_F ratio of 250, 1300, and 140, respectively (note that a factor $\sqrt{2}$ has been applied to the first ratio to take into account that mirrors make a 45° angle with respect to the beam propagation direction). Practically, the Fresnel number is calculated at the iris location as long as its aperture is less than 4 mm and at the crystal position otherwise. In the latter case, \mathcal{N}_F is fixed at its maximum value, here 140. Note that an adequate choice of f and L allows us to reach values up to $\mathcal{N}_F=200$.

In addition to the cavity boundary conditions discussed above, the optical oscillator is also sensitive to the bulk symmetry σ_u , which mainly results from the interplay of the beam propagation along the cavity axis with the transverse coordinates. For instance, in a ring cavity with an odd number of mirrors, σ_u may be D_2 or D_4 , while it is $O(2)$ with an even number of mirrors. More generally, each time the ratio R_ν takes a rational value, a degeneracy of modes appears that can create locally a symmetry different from $O(2)$. For example, with $R_\nu=2$ (confocal cavity), all modes with central symmetry (antisymmetry) are degenerated. Let us stress that σ_0 and σ_u are very different and that one of them does not belong *a priori* to a subgroup of the other. For instance, σ_0 and σ_u may have different symmetry axes as, e.g., when the cavity and the iris are not coaxial.

In this system, parameters such as the cavity alignment, the shape of the iris, and the ratio between longitudinal and transverse mode spacings may alter σ_u or σ_0 . Other parameters such as the gain and the cavity length do not act on them, although they do on the observed patterns. As we want to stress the pertinence of symmetry properties on the dynamics, our approach consists in identifying and characterizing the most ordered pattern for given σ and \mathcal{N}_F , whatever the gain and the cavity length. In addition, we perform this study on time-averaged patterns, as spontaneous symmetry breaking often appears associated with a temporal bifurcation. As mentioned earlier, using time-averaged rather than instantaneous patterns restores underlying symmetries [4,5].

At low Fresnel number, typically $\mathcal{N}_F < 5$, it has already been shown that the OPG exhibits simple time behaviors, typically stationary or periodic, easily interpreted through expansion on the Gaussian modes of the empty cavity [6,7]. For example, for $\sigma_0 = \sigma_u = O(2)$, a typical observed pattern involves vortices rotating around a common center [7]. Therefore, the $O(2)$ symmetry is broken in the instantaneous pattern. In this case, it is trivial that time averaging restores the cylindrical symmetry. On the contrary, if either σ_u or $\sigma_0 = D_4$ (rectangular symmetry), patterns no longer exhibit a cylindrical symmetry, even on average [6]. This behavior appears to be general at small Fresnel numbers, where the competition between σ_u and σ_0 leads the system to follow the lowest symmetry.

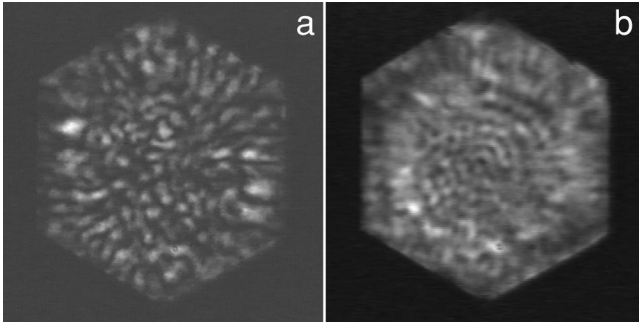


FIG. 2. Patterns obtained in an OPG with $\mathcal{N}_F \approx 10$, $\sigma_u = O(2)$, and hexagonal boundaries: (a) snapshot and (b) average on four periods.

The OPG patterns have been reconsidered using the symmetry point of view developed above for increasing Fresnel number starting from the low-value domain. Figure 2 shows as an example a typical pattern obtained at $\mathcal{N}_F \approx 10$ with $\sigma_0 = D_6$ (hexagonal iris) and $\sigma_u = O(2)$ but different symmetry axes. The instantaneous pattern [Fig. 2(a)] is disordered, but time averaging of the pattern [Fig. 2(b)] reveals the underlying order, as spots distributed on rings are clearly visible. Figure 3 shows the scaling laws of this pattern obtained from an azimuthal spatial averaging of the time-averaged intensity distribution. Figure 4 is a plot of the number N of minima along a diameter $2R$ versus \mathcal{N}_F for different values of cavity length and σ_0 , with $\sigma_u = O(2)$. For $\mathcal{N}_F < \mathcal{N}_{F_1} \approx 19$, the number of minima is approximately equal to \mathcal{N}_F , as predicted for Gaussian modes. As a consequence, it appears that in this \mathcal{N}_F range, the output patterns of the OPG are determined by both the iris and the cavity geometry and follow scaling laws of the empty cavity modes. Similar results were found for the CO_2 laser [8,9] and interpreted as a consequence of the interaction between a small number of modes [9]. In the present case, the patterns are also likely to be composed of a small number of modes, selected by a process of transverse spatial hole burning, as in [9].

Figure 4 shows a drastic change in the scaling law for $\mathcal{N}_F > \mathcal{N}_{F_1}$. N still varies linearly with \mathcal{N}_F , but now with a slope much smaller than 1. This regime is associated with

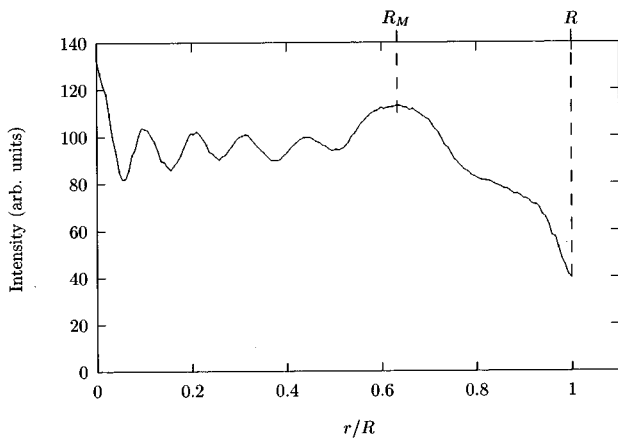


FIG. 3. Spatial average intensity of the pattern of Fig. 2 as a function of the distance to the center of the pattern.

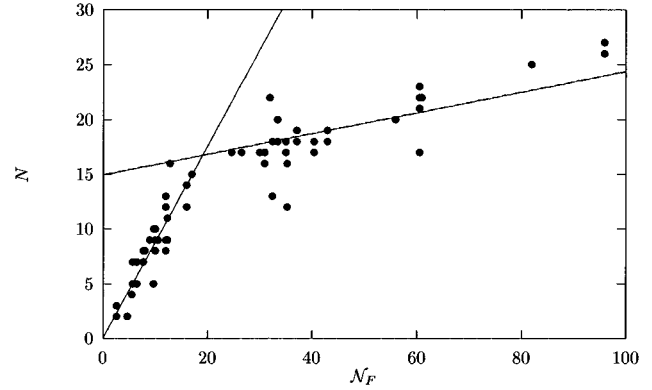


FIG. 4. Number of minima N deduced from plots as shown in Fig. 3, versus Fresnel number \mathcal{N}_F . The dots correspond to experimental results. The two straight lines, of equation $\alpha N + \beta$ with $\alpha = 0.90$ and $\beta = 0.01$ ($\alpha = 0.09$ and $\beta = 15$), result from a fit on the values of N obtained for $\mathcal{N}_F < \mathcal{N}_{F_1}$ ($\mathcal{N}_F > \mathcal{N}_{F_1}$) with $\mathcal{N}_{F_1} \approx 19$.

alterations in the shape of the pattern: The organization at the center of the time-averaged pattern becomes different from that at its edges. Moreover, this arrangement is independent of σ_0 and is related to σ_u only. This behavior is illustrated in Figs. 2 and 3, although it remains weak at such low \mathcal{N}_F . In these patterns, the hexagonal external shape is that of the iris, showing no simple ordered structure, while the central area is typical of $\sigma_u = O(2)$. As \mathcal{N}_F increases, an intermediate bordering disordered area appears between $r = R_M$ and $r = R$ (Fig. 3). This *outer* area appears whatever the shape of the iris and thus also for $\sigma_0 = O(2)$. In these conditions, σ_u and σ_0 have different actions: The former determines the order of the *inner* area of the time averaged pattern, while the latter rules the *outer* area.

The change in the slope of the plot of Fig. 4 is associated with a relative decrease of the number of rings versus \mathcal{N}_F as compared with the low- \mathcal{N}_F behavior. A check in scaling laws indicates that this change originates from an increase of the average distance between rings and not from an enlargement of the disordered outer zone $R - R_M$. In addition to the $N = \mathcal{N}_F$ scaling law, Gaussian modes also obey a $R_M/w = \sqrt{\mathcal{N}_F}$ scaling, where w is the spot size of the fundamental mode. The plot of R_M/w versus $\sqrt{\mathcal{N}_F}$ as shown in Fig. 5 does not present any variation in the domain around \mathcal{N}_{F_1} : A least-square fit on a straight line gives a slope approximately equal to 1. Therefore, the transition at \mathcal{N}_{F_1} appears to originate from an increase of the average distance between the rings of the patterns.

From the modal point of view, this can be easily explained if one considers that, as the number of modes increases, including modes from different orders, the pattern becomes spatially quasiperiodic, forming some kind of Moiré pattern. This explains the change in the slope of Fig. 4.

To understand the meaning of this transition from the symmetry point of view, we have plotted the relative size of the inner zone, where σ_u dominates, as a function of \mathcal{N}_F (Fig. 6). It appears clearly that the inner part, which covers initially a negligible part of the whole pattern, increases until it reaches an asymptotic value of about 80% around \mathcal{N}_{F_1} .

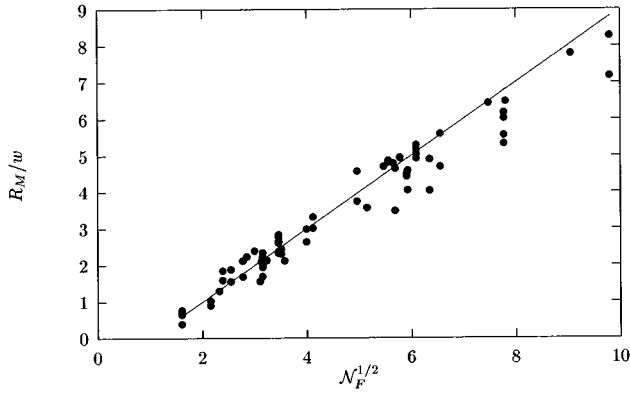


FIG. 5. Normalized distance R_M/w between the center of the pattern and the last ring as a function of $\mathcal{N}_F^{1/2}$. The $R_M/w = \mathcal{N}_F^{1/2} - 1$ straight line has been plotted as a reference.

Therefore, the transition at \mathcal{N}_{F_1} appears as a change in the relative influence of σ_0 and σ_u . Starting from low \mathcal{N}_F , the range of action of σ_u extends progressively and eventually σ_0 becomes marginal.

The first transition is the equivalent of that reported in [2], where the transition was observed on vortices through their total imbalance and their average separation distance. Using average patterns, information on the symmetries is kept: A transition occurs from a regime dominated by the bulk symmetry, linked to the cavity, towards one ruled by the boundary symmetry, linked to the external shape of the cavity. Thus it appears that this transition does not correspond to a brutal loss of influence of the cavity on the behavior as suggested in [2]. The transition here is also different from that observed in [5] in the Küppers-Lortz instability because of the existence of σ_u : Indeed, beyond \mathcal{N}_{F_1} , no symmetry is lost in the OPG, while it is the case in [5].

As the Fresnel number increases, the pattern evolution is monitored through the contrast in the ring intensities as revealed by the spatial averaged intensity of the time-averaged patterns. The contrast decreases above the first transition and finally almost vanishes for $\mathcal{N}_F > \mathcal{N}_{F_2}$ with $\mathcal{N}_{F_2} \approx 100$, leading to a flat curve. This behavior is illustrated in Fig. 7, where the maximum amplitude ΔI of the inner zone of the patterns

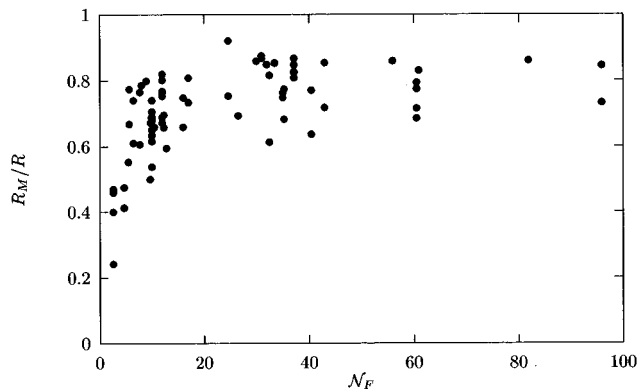


FIG. 6. Relative distance R_M/R between the center of the pattern and the last ring as a function of the Fresnel number.

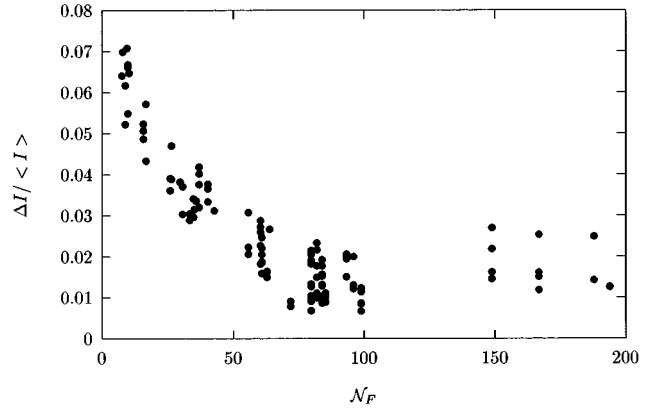


FIG. 7. Intensity variations ΔI appearing in spatial averaged plots as a function of \mathcal{N}_F . Long-range variations have been removed.

is plotted versus the Fresnel number. Note that, for $\mathcal{N}_F > \mathcal{N}_{F_2}$, the small variations, of the order of 2% of the mean intensity, which are observed at large Fresnel numbers, are due to the noise remaining after the averaging a limited number of data.

This evolution is due to the loss of any order in the pattern so that the dynamics no longer depends on σ_u . The hypothesis of a spatial rearrangement of the pattern, corresponding to a different ordered structure, may be ruled out since a plot of the amplitude variations of the time-averaged two-dimensional patterns, without spatial averaging, shows the same behavior. This interpretation is reinforced by the fact that the spatial modulation of the instantaneous patterns does not vary significantly with \mathcal{N}_F .

Several levels of spatiotemporal disorder can be defined as a function of the relative value of the transverse wavelength λ_T as compared to the correlation length l_c of the pattern dynamics. When $\lambda_T \approx l_c$, the information propagates over a distance large enough to make possible long-range correlations. On the contrary, when $\lambda_T \gg l_c$, long-range correlations disappear. In the former case, behaviors are often referred to as spatiotemporal chaos, while in the latter one speaks of turbulence. The transition in \mathcal{N}_{F_2} appears as a loss of long-range spatial order and so could be considered as a transition from spatiotemporal chaos to turbulence. Although a direct analysis of the temporal dynamics should be performed before concluding this point, it is worthwhile to evaluate here the order of magnitude of λ_T at the second transition point \mathcal{N}_{F_2} and compare it with the typical length scales of the setup. In optical oscillators, it is generally assumed that λ_T is approximately equal to the average distance between two successive intensity maxima of the Gaussian modes and so evolves as $w/\sqrt{\mathcal{N}_F}$. As our cavities are built so that the waist of the beam w_0 is inside the photorefractive crystal, l_c is approximately equal to $w_0/\sqrt{\mathcal{N}_F}$, which gives for our typical cavities $l_{c_2} \approx 25 \mu\text{m}$ at \mathcal{N}_{F_2} . Here the correlation length l_{c_2} has been estimated within the spatial resolution of our data acquisition system to be equal to the period Λ of the optical grating in the crystal. Although Λ is not usually considered as an important space scale in the OPG, here it seems to play the role of the correlation length of the

dynamics and thus the second transition appears as a transition to turbulence.

To summarize, the route to turbulence in the OPG looks like a competition between two symmetries, governing the spatial organization of the edge and the central area, respectively. As the aspect ratios increase, two successive transitions lead from order to turbulence: The first one appears as a change in the leading symmetry, namely, from that determined by the transverse boundaries to that determined by the bulk geometry; the second transition appears as a complete loss of long-range correlations and occurs as the transverse wavelength of the pattern becomes smaller than the grating period in the crystal, which fixes the correlation length of our system. In this case, the bulk symmetry loses also any influence on the patterns geometry and a more developed turbulence appears. Thanks to the flexibility of optical systems, in particular concerning changes in boundary conditions, the separation of the roles played by the various symmetries of our system has allowed one to uncover details of the transition to turbulence in optics. Experiments in Faraday waves

[4], rotating Rayleigh-Bénard convection [5], or lasers [3] show that this behavior could be generic and probably stand in any system involving symmetries originating in different spatial elements. In particular, it has been shown that the OPG could be modeled as a class-A laser, i.e., near the threshold with a complex Swift-Hohenberg or a complex Ginzburg-Landau equation where the order parameter is the electric field [10]. Therefore, the next step in this study should be to look for these transitions to turbulence in such a model and evaluate whether such a behavior is universal. The experimental methods described here could also be tested in other fields of physics.

We acknowledge Neal Abraham and Gilbert Grynberg for useful discussions. The Laboratoire de Spectroscopie Hertzienne is “Associé au CNRS” and a member of the Centre d’Etudes et de Recherches Lasers et Applications (CERLA). The Région Nord-Pas-de-Calais and the European Community are gratefully acknowledged for their financial support through the CERLA.

-
- [1] See, e.g., J. Lega, J. V. Moloney, and A. C. Newell, *Physica D* **83**, 478 (1995).
- [2] F. T. Arecchi, S. Boccaletti, P. L. Ramazza, and S. Residori, *Phys. Rev. Lett.* **70**, 2277 (1993).
- [3] C. Green, G. B. Mindlin, E. J. D’Angelo, H. G. Solari, and J. R. Tredicce, *Phys. Rev. Lett.* **65**, 3124 (1990).
- [4] B. J. Gluckman, P. Marcq, J. Bridger, and J. P. Gollub, *Phys. Rev. Lett.* **71**, 2034 (1993).
- [5] L. Ning, Y. Hu, R. E. Ecke, and G. Ahlers, *Phys. Rev. Lett.* **71**, 2216 (1993).
- [6] D. Hennequin, L. Dambly, D. Dangoisse, and P. Glorieux, *J. Opt. Soc. Am. B* **11**, 676 (1994).
- [7] D. Hennequin, L. Dambly, D. Dangoisse, and P. Glorieux, *J. Phys. III* **4**, 2459 (1994).
- [8] M. Brambilla, M. Cattaneo, L. A. Lugiato, R. Pirovano, F. Prati, A. J. Kent, G. L. Oppo, A. B. Coates, C. O. Weiss, C. Green, E. J. D’Angelo, and J. R. Tredicce, *Phys. Rev. A* **49**, 1427 (1994).
- [9] E. Louvergneaux, D. Hennequin, D. Dangoisse, and P. Glorieux, *Phys. Rev. A* **53**, 4435 (1996).
- [10] K. Staliunas, M. F. H. Tarroja, G. Slekys, C. O. Weiss, and L. Dambly, *Phys. Rev. A* **51**, 4140 (1995).